Modeling the climatic implications and indicative senses of the Guliya $\delta^{18}O$ temperature record to the ocean-atmosphere system during the past 130 ka

Dong Xiao[1], Ping Zhao[2], Yue Wang[3] and Xiuji Zhou[1, 4]

[1]Chinese Academy of Meteorological Sciences, Beijing 100081, China

[2]National Meteorological Information Center, Beijing 100081, China

[3]State Key Laboratory of Marine Geology, Tongji University, Shanghai 200092, China

[4]State Key Laboratory of Severe Weather, Beijing 100081, China

Corresponding author: Ping Zhao E-mail: zhaop@cma.gov.cn

Running title: Modeling climatic implications of the Guliya $\delta^{18}O$ temperature record

Abstract

Using an intermediate-complexity UVic Earth System Climate Model (UVic Model), the geographical and seasonal implications and an indicative sense of the historical climate found in the Guliya $\delta^{18}O$ ice core record (hereinafter, the Guliya $\delta^{18}O$) are investigated under a time-dependent astronomical forcing with an acceleration factor of 100 over the past 130 ka. The results reveal that the simulated August–September Guliya surface air temperature (SAT) reproduces the 21-ka precession and 43-ka obliquity cycles of the Guliya $\delta^{18}O$, showing an in-phase variation with the latter. Moreover, the Guliya $\delta^{18}O$ may be also an indicator of the August–September Northern Hemispheric (NH) SAT. Corresponding to the warm and cold phases of the precession cycle in the Guliya August–September SAT, there are two anomalous patterns in SAT and sea surface temperature (SST). The first anomalous pattern shows an increase of SAT (SST) toward the Arctic, which is possibly associated with an increase of the NH incoming solar radiation that is caused by the in-phase superposition between the precession and obliquity cycles. The second anomalous pattern shows an increase of SAT (SST) toward the equator, which is possibly due to a decrease of incoming solar radiation over the NH polar which result from the anti-phase counteraction between the precession and obliquity cycles. The summer (winter) Guliya and NH temperatures are higher (lower) in the warm phase of the August–September Guliya than in its cold phase. Moreover, in August–September, the Guliya SAT is closely related to the North Atlantic SST, in which the Guliya precipitation may act as a "bridge" linking the Guliya SAT and the

North Atlantic SST.

Keywords: Guliya $\delta^{18}O$, UVic Model, climatic implication, precession, obliquity

1. Introduction

Compared to other proxy data, ice core records offer long-time-scale, continuous, and high-resolution climatic and environmental records of many informational parameters (Yao and Wang, 1997). Among the long-term ice core records, the Guliya ice cap, located in a northern subtropical region, is the largest (with a total area of 376.1 km^2), the highest (with an elevation of 6,700 m), and the thickest (with an average thickness of approximately 200 m and a maximum thickness of approximately 350 m) ice body found in the middle and low latitudes of the Northern Hemisphere (NH) (Yao et al., 1994; Yao et al., 2000). In 1992, Chinese and American scientists drilled into the Guliya glacier in the North Tibetan Plateau at 81.5°E, 35.2°N and retrieved three ice cores with lengths of 34.5, 93.2, and 308.6 m. The stable oxygen isotope records inside these ice cores constitute reliable indicators of environmental changes (Li et al., 2000). The environmental changes over the past 130 ka are recorded as fluctuations in the concentration of oxygen-18 ($\delta^{18}O$) in precipitation found in the Guliya ice core (hereinafter referred to as the Guliya $\delta^{18}O$). The observed monthly $\delta^{18}O$ in the Guliya precipitation is well correlated with the local monthly surface air temperature (SAT) (Yao et al., 1996a). They found that moisture source is identified as a major factor in the spatial distribution of $\delta^{18}O$, but air temperature determines the temporal fluctuations of $\delta^{18}O$ at the meteorological stations at the northern Tibetan Plateau. Therefore, the Guliya $\delta^{18}O$ record is often considered to be representative of the temperature of the Tibetan Plateau (Yao et al., 1995; Yao et al., 1996a), which witnessed significant warm and cold periods, either in

the interglacial stage or in the glacial stage, over the past 130 ka. The alternation of these warm and cold periods indicated an obvious 21-ka cycle (Yao et al., 1997). The Guliya $\delta^{18}O$ has been used to investigate the features of the Younger Drays and Heinrich events and to compare with the Arctic and Antarctic records (Yang et al., 1997), and has also been used as a temperature index to investigate temporal structures over many periods including the orbital and sub-orbital scales, the millennial scale, the century scale, the decadal scale, and others (Yao et al., 1996b; Yao et al., 1997; Shi et al., 1999; Yao et al., 2001). Therefore, Guliya ice cores offered a new way to understand the environmental changes of the third Pole—Tibet Plateau and is also helpful for understanding the effects of climate changes in the middle and low latitudes.

In the context of the Milankovitch astronomic climate theory (Milankovitch, 1969), the latitudinal and seasonal distributions of incoming solar radiation induced by the astronomical parameters (precession, obliquity, and eccentricity) are the most probable driving forces for the orbital-scale climate changes and glacial cycles. For example, Yao et al. (1997) examined the relationship between June incoming solar radiation at 60°N and the Guliya $\delta^{18}O$ and found that the appearance of 21-ka cycles in the Guliya $\delta^{18}O$ indicates a close connection of Guliya $\delta^{18}O$ with the astronomical parameters. The former led to the latter approximately one-quarter phase of the precession cycle (5 ka), which indicated the drive of incoming solar radiation on the Guliya $\delta^{18}O$ record. Due to the seasonal and latitudinal asymmetries of incoming solar radiation induced by the precessional motion (Milankovitch, 1969; Berger, 1978), the

Guliya $\delta^{18}O$ temperature record, as a response to the incoming solar radiation, possibly contain climate signals in particular seasons and latitudes and the variations of these astronomical parameters possibly exert influences on variability of the Guliya $\delta^{18}O$ (Yao et al., 1997).

Although the Guliya $\delta^{18}O$ record, which is used to indicate the local temperature, have been extensively investigated, the seasonal and spatial climate ranges represented by the Guliya $\delta^{18}O$ and the climatic relationship on longer timescales between the Guliya $\delta^{18}O$ and ocean-atmosphere system remain unclear (Zhang et al., 1995; Yao et al., 1996a). For example, what season SAT does the Guliya $\delta^{18}O$ temperature record indicate? Are the ocean and atmosphere systems related to variability of the Guliya $\delta^{18}O$? If yes, what are the possible physical processes responsible for this link? With these questions in mind, we employ an intermediate-complexity coupled ocean-atmosphere climate model to understand the geographical and seasonal implications and the indicative properties of the Guliya $\delta^{18}O$ record with respect to the atmosphere-ocean systems and to discuss the associated physical processes.

The rest of this paper is organized as follows. The model and methods are described in Section 2. A comparison between $\delta^{18}O$ temperature record and the simulated SAT in Guliya are investigated in Section 3 to determine in which season the simulated Guliya SAT is consistent with the Guliya $\delta^{18}O$ temperature record. The indicative senses of the Guliya SAT to the simulated ocean-atmosphere system in August–September are explored in Section 4. The relation between Guliya $\delta^{18}O$ and

August–September ocean-atmosphere system and associated physical processes are discussed in Section 5. A summary and a discussion are presented in Section 6.

2. Model and methods

This study employs version 2.9 of the UVic Earth System Climate Model (UVic Model) with a resolution of 3.6° in longitude and 1.8° in latitude. The UVic Model is an intermediate-complexity coupled atmosphere-ocean model (Weaver et al., 2001) in which the atmospheric model comprises a single-layer energy-moisture balance model and the ocean component utilizes version 2.2 of the GFDL Modular Ocean Model with 19 vertical levels. The UVic Model can capture several major features of global surface temperature and precipitation and has been widely used in paleoclimate research (Weaver et al., 2001; Matthews et al., 2004; Stouffer et al., 2006; Weber et al., 2007; Fyke et al., 2011). Moreover, the UVic Model can also reproduce variations of temperature in China and the NH during the past millennium (Xiao et al., 2012).

Equilibrium simulations are often used to provide "snapshots" of the equilibrium climate for a prescribed insolation or astronomical parameter (Kutzbach, 1981; Hewitt and Mitchell, 1998; Montoya et al., 2000; Liu et al., 2006). Such equilibrium simulations are unable to simulate the forcing effects of the varying astronomical parameters on the climate system. Thus, transient simulations are employed to investigate influences of varying astronomical parameters on climate (Lorenz and Lohmann, 2004; Kutzbach et al., 2008). However, it is difficult to simulate a period of one hundred thousand years using the complicated coupled models to explore climate

responses to astronomical forcing. Some authors applied integrated acceleration schemes in transient paleoclimate simulations (Jackson and Broccoli, 2003; Timm and Timmermann, 2007; Timmermann et al., 2007; Kutzbach et al., 2008). Lorenz and Lohmann (2004) showed that acceleration factors of 10 and 100 yield similar results. Timm and Timmermann (2007) compared advantages and disadvantages of the acceleration technique and found out that a large deviation of the accelerated simulation from the non-accelerated simulation mainly occurs in the Southern Ocean, in regions of deep-water formation, large thermal inertia, and below the thermocline, while it is little in SAT and surface sea temperature (SST). In the present study, we focus on the indicative senses of the Guliya $\delta^{18}O$ in the mid and low latitudes.

The used time-dependent astronomical forcing (due to changes in longitude of perihelion, axial tilt and eccentricity) is calculated according to Berger (1978). The UVic Model has first been spun up for 200 model years under the prescribed astronomical forcing. Then, we accelerate the astronomical forcing by a factor of 100, i.e., the astronomical parameters are advanced by 100 years at the end of each year in the simulation. The other climate forcings, such as ice sheets, greenhouse gas concentration and solar insolation (solar constant) are set to the constants at the year 2000 AD through the entire simulation. The accelerated simulation runs from 130.8 ka BP to the present. The 1308 time samples (corresponding to the period from 130.8 ka BP to the present) of the model output are analyzed in this study.

The modeled SAT over the Guliya region is an average over 80–85°E, 33–38°N. Because there are 1308 model years in this simulation, the Guliya $\delta^{18}O$ data with 1875

samples during the past 130 ka obtained from Yao et al. (1997) are linearly interpolated over the 1308 model years. The smoothness of the time series of an approximately 51-yr moving mean of the Guliya $\delta^{18}O$ is similar to that of the simulated August–September (see section 3) Guliya SAT. For the 51-yr moving mean time series over 1308 years, their effective free degree decrease and the significant critical value of correlation coefficient will increase. Therefore, a Monte Carlo Simulation gives the critical value of the correlation coefficient at the 95% confidence level as 0.26. The monthly mean SAT from the Climate Research Unit (CRU) analysis with a horizontal resolution of 0.5°×0.5° during 1901–2009 (Mitchell and Jones, 2005) is used to compare the annual cycle between the CRU analysis data and the simulated SAT in Guliya.

Correlation and composite analyses are applied to examine the relationships between pairs of variables. Lagging and leading correlations and a squared wavelet coherence analysis (Grinsted et al., 2004) are employed to examine the phase relationships between different variables. A power spectrum analysis is performed to display the periods of the Guliya $\delta^{18}O$ record using the REDFIT software in MATLAB (Schulz and Mudelsee, 2002).

3. A comparison between $\delta^{18}O$ temperature record and the simulated SAT in Guliya

The Guliya $\delta^{18}O$ experienced several approximately 21-ka cycles in the past 130 ka that are directly related to precession (Yao et al., 1997). However, the incoming

solar radiation, as a forcing of the Guliya $\delta^{18}O$, differs between the twelve months of the year due to precessional motion (Milankovitch, 1969; Berger, 1978). Thus, we first examine annual cycle of the Guliya incoming solar radiation. Figure 1a shows the annual cycle of the Guliya incoming solar radiation anomaly in the past 130 ka. In this figure, the annual cycle of the Guliya incoming solar radiation anomaly exhibits approximately eleven vertical belts toward the right, with a varying range of approximately 75 W m^{-2}, and the largest variability of incoming solar radiation generally occurs in May. Moreover, the incoming solar radiation anomaly also shows a weakening trend over the past 130 ka and is much weaker from 60 ka BP to the present, which might be due to a smaller variation of precessional motion during this period (Figure not shown) that is modulated by a smaller eccentricity according to the astronomic climate theory (Milankovitch, 1969; Berger, 1978).

Corresponding to the variation of incoming solar radiation over the Guliya region, the annual cycle of the Guliya SAT anomaly also exhibits the similar eleven vertical belts toward the right, with a lifetime similar to the 21-ka precession cycle, and the Guliya SAT anomaly is also weaker from 60 ka BP to the present (Fig. 1b). Such variations of the Guliya SAT anomaly could be well explained by those of incoming solar radiation. Meanwhile, the largest Guliya SAT anomaly, which varies in magnitude by approximately 6 °C, generally occurs in June, one month later compared to the largest incoming solar radiation anomaly. This delayed response of SAT to incoming solar radiation in the Guliya region indicates a possible forcing of the latter to the former in the past 130 ka. Then, are the incoming solar radiation and

SAT anomalies in the Guliya region indicated by the Guliya $\delta^{18}O$ temperature record?

Because the phase of the precession cycle of June incoming solar radiation at 60°N is approximately one-quarter phase ahead of that in Guliya $\delta^{18}O$ (Yao et al., 1997), the variability of the Guliya $\delta^{18}O$ temperature record is possibly synchronous with the variation of the simulated Guliya SAT in a certain month that lags to the June incoming solar radiation. Here, we examine the relationship between the Guliya $\delta^{18}O$ temperature record and the simulated Guliya SAT from June to December. Figure 2 presents the correlation coefficients between the Guliya $\delta^{18}O$ and the simulated Guliya monthly mean SAT from June to December, respectively. In this figure, the positive correlation coefficient gradually increases from June to August and there are positive correlation coefficients of 0.43 in August and 0.4 in September (both significant at the 99% confidence level), with no significant correlation coefficient (not exceeding the 95% confidence level) in the others months. This result implies that the Guliya $\delta^{18}O$ temperature record closely connects to the simulated SAT in August and September. Figure 3 further presents the time series of the Guliya $\delta^{18}O$ and the simulated August–September Guliya SAT. Both generally present an approximately 21-ka precession cycle and an in-phase relationship during the majority of the 130 ka (except in 45–20 ka), in which the first, second, third, fourth, and sixth peaks of the simulated Guliya SAT and the first, second, and third valleys of the SAT generally correspond to those of the Guliya $\delta^{18}O$. The correlation analysis exhibits a positive correlation coefficient of 0.47 between the Guliya $\delta^{18}O$ temperature record and the simulated August–September SAT, significant at the 99.9% confidence level.

In brief, the simulated August–September Guliya SAT is well correlated to the Guliya $\delta^{18}O$, and generally captures the 21-ka precession of the Guliya $\delta^{18}O$.

To understand whether the simulated August–September SAT captures the varying periods of the $\delta^{18}O$ temperature record in Guliya, we perform a power spectrum analysis (Fig.4). The result reveals three periods of the Guliya $\delta^{18}O$ record. The first is at 43.6 ka (significant at the 99% confidence level), the second is at 20.762 ka (significant at the 99% confidence level), and the third is at 10.634 ka (a peak of red noise) (Fig. 4). It is evident that the first two periods correspond to the periods of the precession and the obliquity, respectively, which indicates the possible controls of precessional motion and obliquity variation on the Guliya $\delta^{18}O$ over the past 130 ka. The similar periods (43.599 ka, 22.947 ka, and 11.179 ka) are also detected in the simulated Guliya August–September SAT (figure not shown) and the precession cycle in both the simulated Guliya August–September SAT and the Guliya $\delta^{18}O$ temperature record is more obvious than the obliquity cycles. Moreover, we also analyze the squared wavelet coherence between the Guliya $\delta^{18}O$ and the simulated August–September Guliya SAT (Fig. 5). In this figure, the arrows at the period of 21-ka precession generally point rightward and upward before 60 ka BP and afterwards point rightward and downward and the arrows at the period of 43-ka obliquity point rightward and upward during the entire 130 ka. These results show the arrows toward the right generally, indicating an in-phase relationship between the Guliya $\delta^{18}O$ and the simulated local August–September SAT at the periods of 21-ka precession and 43-ka obliquity, further supporting the result from Fig. 3.

The foregoing analyses show that the Guliya $\delta^{18}O$ temperature record mainly reflects the variability of the local August–September SAT. The consistency in periods (21-ka precession and 43-ka obliquity) and phase between the simulated August–September Guliya SAT and the Guliya $\delta^{18}O$ temperature record also demonstrates the reliability of the simulated August–September Guliya SAT.

4. Indicative senses of Guliya SAT to the simulated ocean-atmosphere system in August–September

As noted in above section, the 21-ka precession cycle of the Guliya $\delta^{18}O$ and the simulated August–September Guliya SAT is stronger, while its 43-ka obliquity cycle is weaker. Thus we focus on the indicative senses of the Guliya SAT to SAT and SST between the warm and cold phases of the 21-ka precession cycle of the simulated August–September Guliya SAT. According to Fig. 3, we use respectively five highest (11–6, 33–28, 59–54, 83–78, and 105–100 ka BP; called the warm phase) and lowest (23–18, 45–40, 72–67, 94–89, and 117–112 ka BP; called the cold phase) periods of the August–September Guliya temperature to perform a composite analysis between warm and cold phases.

4.1 Indicative sense to the simulated August–September SAT

Figure 6a displays the composite difference of the simulated August–September SAT between 11–6 ka BP and 23–18 ka BP (11–6 ka BP minus 23–18 ka BP), which corresponds to the difference between the early Holocene and the Last Glacial

Maximum. Compared with the cold phase in 23–18 ka BP, the SAT in the warm phase during 11–6 ka BP is significantly warmer over the NH, and large temperature anomalies occur over the Asian and African continents, with a maximum value of approximately 1.4°C. The temperature anomalies over the Southern Hemisphere (SH) and the ocean are weaker than those over the NH and land. The anomalies generally increase toward the Arctic. A similar anomalous pattern also occurs between 59–54 ka BP and 72–67 ka BP (Fig. 6c), and between 105–100 ka BP and 117–112 ka BP (Fig. 6e); that is, there are higher (lower) temperature anomalies over the NH (SH) when the August–September Guliya SAT is higher.

However, another anomalous pattern in SAT also occurs between the high and low Guliya August–September SAT cases. Figure 6b presents the composite difference in SAT between 33–28 ka BP and 45–40 ka BP. In this figure, the SAT anomalies generally show an increase toward the equator, and relative to 45–40 ka BP, the SAT in 33–28 ka BP was warmer over the majority of regions except the NH high latitudes, with anomalous warm centers above 1.2 °C in Africa and South America. A similar anomalous pattern is also observed in Fig. 6d. This result reveals an alternation (with an approximately 43-ka cycle) of two anomalous SAT patterns between the warm and cool phases of the precession cycle of the Guliya August–September SAT. Then, why do these two anomalous SAT patterns occur and alternate with a period of approximately 43-ka?

The previous study showed that the 43-ka obliquity cycle significantly modulates the earth's climate, especially at high latitudes (Short et al., 1991), and the latitudinal

inhomogeneity of incoming solar radiation may be caused by the precessional motion. Thus, the two anomalous patterns of SAT are associated with not only the precession cycle but also the obliquity cycle. To understand the contributions of the precession and obliquity cycles to these two anomalous patterns, following Yin and Berger (2010; 2012), we examine the temporal evolutions of the obliquity and the simulated Guliya SAT (indicating the local influence of precession). Figure 7 shows the temporal curves for the obliquity and the simulated August–September Guliya SAT during the past 130 ka. For the first type of the anomalous SAT pattern (shown in Figs. 6a, c, and e), the precession minima (maxima) in the simulated Guliya SAT is more or less synchronous with the obliquity minima (maxima), which strengthens the August–September incoming solar radiation in the NH. For the second type of the anomalous SAT pattern (shown in Figs. 6b and d), there is a general anti-phase relationship between the precession minima (maxima) in the simulated Guliya SAT and the obliquity maxima (minima), which weakens the incoming solar radiation in the NH high latitudes. It is evident that the first anomalous SAT pattern may result from the in-phase superposition between the precession and obliquity cycles and the second anomalous SAT pattern may be due to the anti-phase counteraction between the precession and obliquity cycles. The alternation of these two anomalous SAT patterns with approximately 43-ka cycles may be associated with the obliquity cycle. Thus, the simulated Guliya SAT may indicate the in-phase and anti-phase varying features of SAT in 21-ka precession and 43-ka obliquity cycles.

4.2 Indicative sense to annual cycle in Guliya and NH

In this section, we investigate the differences of annual cycle in the simulated Guliya SAT between the warm and cold phases of the 21-ka precession cycle of the simulated Guliya August–September SAT. Firstly, a comparison of the Guliya SAT annual cycle between the 100-year CRU analysis dataset and this simulation shows that the variation of the simulated SAT annual cycle under the astronomical forcing is generally consistent with that of the CRU data. Figure 8 presents the annual cycle of the modeled Guliya SAT in warm and cold phases and their differences. In the figure, the annual cycle shows the similar features for each warm phase and each cold phase, with the highest temperature in June and July and the lowest temperature in December and January. Compared with the cold phase, the Guliya SAT in the warm phase is generally higher in the warm season (May–September) and lower in the cold season (October–April) (Fig. 8a, c–e), which indicates a larger seasonal variation in the warm phase than in the cold phase. For example, the annual range of July (January) temperature between the warm and cold phases varied from 0.5 (0) °C (Fig. 8b) to 4 (2) °C (Fig. 8e). This result exhibits a larger temperature difference between the warm and cold phases in summer than in winter. Moreover, it is also seen from Fig. 8 that the difference of the annual cycles in the Guliya SAT between the warm and cold phases of the August–September Guliya SAT shows the similar feature, which suggests the little influence of the obliquity cycle on the annual cycle of the Guliya SAT. Our analysis further reveals the similarly varying feature of the simulated NH temperature. Therefore, the warm-season (cold-season) Guliya and NH temperatures

are higher (lower) in the warm phase of the Guliya SAT than in its cold phase.

4.3 Indicative sense to the simulated August–September SST

Consistent with SAT, the SST anomalies between the warm and cold phases also show two anomalous patterns. One occurs between 11–6 ka BP and 23–18 ka BP (Fig. 9a), between 59–54 ka BP and 72–67 ka BP (Fig. 9c), and between 105–100 ka BP and 117–112 ka BP (Fig. 9e). This pattern is characterized by a warmer NH ocean and a cooler SH ocean, with SST increasing toward the Arctic. Another pattern occurs between 33–28 ka BP and 45–40 ka BP (Fig. 9b) and between 83–78 ka BP and 94–89 ka BP (Fig. 9d), with a warmer SST at the middle and low latitudes and a cooler SST at the high latitude, which indicate an increasing SST toward the equator. The alternation of two anomalous SST patterns also displays an approximately 43-ka obliquity cycle. Similar to SAT, the first anomalous SST pattern may be due to the contributions of accumulation of the precession and obliquity cycles, which increase the August–September incoming solar radiation in the NH, while the second anomalous SST pattern is induced by the anti-phase counteraction between the precession and obliquity cycles, which decrease the August–September incoming solar radiation over the NH high latitudes.

5. Relation between the Guliya $\delta^{18}O$ and the simulated ocean-atmosphere system and possible physical processes

It is seen from section 3 that the Guliya $\delta^{18}O$ temperature record may reflects the

variation of the local August–September SAT. Here, we further focus on the relationship between the Guliya $\delta^{18}O$ temperature record and the simulated August–September SAT and SST. Figure 10 illustrates the distribution of correlation coefficients between the Guliya $\delta^{18}O$ and the simulated August–September SAT. In this figure, significant positive correlation coefficients cover the majority of the NH, exceeding 0.48 at the latitudes of 45°–80°N and 0.54 over the Bering Strait and the North Atlantic. This result implies that the Guliya $\delta^{18}O$ can better indicate the NH SAT in the middle-high latitudes than in the lower latitudes. Thus, although the Guliya $\delta^{18}O$ is identified as a temperature index of the Tibet Plateau (Yao et al., 1996a), the result of the UVic Model exhibits that the Guliya $\delta^{18}O$ may also represent variability of the August–September NH SAT.

Figure 11 further presents the correlation coefficients between the Guliya $\delta^{18}O$ temperature record and the August–September SST over the past 130 ka. In this figure, significant positive correlation coefficients mainly appear in the North Atlantic, the Bering Sea, the Bay of Alaska, and the Arctic region to the north of Europe, with the maximum correlation coefficient exceeding 0.57 in the North Atlantic. Moreover, the correlation coefficient between the reconstructed equatorial Atlantic SST at 2°30'N, 9°23'E (Weldeab et al., 2007) and Guliya $\delta^{18}O$ is 0.18 (significant at the 90% confidence level), consistent with that (0.21) in Fig. 11, which supports the reliability of the model result. This result also suggests a close link between the Guliya temperature and the Atlantic SST in the past 130 ka. Figure 12a shows the leading and lagging correlation coefficients between the simulated Guliya SAT and the North

Atlantic SST in August–September. It is seen from this figure that the maximum positive correlation occurs near 2.5 ka, which indicates that the simulated Guliya August–September SAT lags the simulated North Atlantic August–September SST by 2.5 ka and a possible effect of the North Atlantic SST on the Guliya SAT. Then, what physical processes are possibly responsible for this influence? One explanation is given below.

Because the $\delta^{18}O$ variable presents in the local precipitation (Yao et al., 1997), the Guliya precipitation may be closely related to the local temperature. Figure 13 illustrates the simulated August–September SAT and precipitation curves in the Guliya region. Both the simulated August–September precipitation and SAT display a significant cycle of approximately 21 ka, and there is an out-of-phase relationship between precipitation and SAT, with a correlation coefficient of –0.95. All the peaks (valleys) in precipitation correspond to valleys (peaks) in SAT. Meanwhile, the strongest negative correlation occurs near 1 ka (Fig. 12b), which indicates that the variation of simulated August–September SAT lags by 1 ka relative to that of the simulated August–September precipitation and suggests that the simulated Guliya precipitation may lead the simulated Guliya SAT in August–September. Several prior studies have shown that the summer North Atlantic SST modulates atmospheric circulation over the NH and affects Asian precipitation on the decadal or longer time scales (Sutton and Hodson, 2005; Dong et al., 2006; Wang et al., 2009; Feliks et al., 2011). Therefore, the anomalous signal from the North Atlantic SST may affect the Guliya SAT and be kept in the Guliya precipitation record. Such an effect leads to a

close link between the Guliya SAT and the North Atlantic SST, in which the Guliya precipitation may act as a "bridge" linking the North Atlantic SST and the Guliya SAT.

6. Summary and conclusion

We employ the UVic Model with the accelerated astronomical forcing by a factor of 100 to examine the climate implications and indicative nature of the Guliya $\delta^{18}O$ temperature record to the ocean and atmosphere systems over the past 130 ka. The result shows that the simulated August–September Guliya temperature generally captures the major varying features and periods (including the 43-ka obliquity and 21-ka precession cycles) of the Guliya $\delta^{18}O$ temperature record, with a correlation coefficient of 0.47 between the Guliya $\delta^{18}O$ and the modeled August–September Guliya SAT. Therefore, the Guliya $\delta^{18}O$ possibly indicate the local August–September SAT. Meanwhile, the Guliya $\delta^{18}O$ may also indicate the simulated NH SAT in these months.

Epochal differences between the warm and cold phases of the Guliya SAT indicate two types of anomalous patterns in SAT and SST. One pattern shows an increase in SAT and SST toward the Arctic, which is due to an in-phase overlap between the precession and obliquity cycles that increases the NH summer incoming solar radiation. Another pattern shows an increase toward the equator, which results from an anti-phase overlap between the precession and obliquity cycles that weakens incoming solar radiation in the NH polar region. In the annual cycle, the Guliya and

NH summer (winter) temperatures are warmer (cooler) in the warm phase of the Guliya August–September SAT than in its cold phase, and the influence of the obliquity cycle on the annual cycle of the Guliya temperature is weaker.

The simulated Guliya temperature is closely related to the simulated North Atlantic SST in August–September, and lags the North Atlantic SST by approximately 2.5 ka and lags the simulated Guliya precipitation by 1 ka. This result suggests an effect of the North Atlantic SST on the Guliya temperature, in which precipitation in Guliya is possibly a "bridge" connecting the local temperature with the North Atlantic SST. However, the UVic Model could not well exhibit atmospheric vertical circulation features. Thus studies from more complex coupled ocean-land-atmosphere models are required in the future. Additionally, climate models may be used to investigate the climate implication and indicative senses in the future work, especially in the spatial scales of the paleoclimate proxy data.

Acknowledgements

We thank constructive comments from two anonymous reviewers, and Prof. Tandong Yao for providing the Guliya ice core data and Dr. Ge Liu for using the software in MATLAB. This work was supported by a major project of the NSFC (40894050), Special Foundation for National Science and Technology Major Project of China (2011FY120300), National Programs for Science and Technology (CHINARE2012-04-04), and the Basic Research Fund of CAMS.

References

Berger, A.: Long-term variations in daily insolation and quaternary climate changes, J Atmos Sci, 35, 2362-2367, 1978.

Dong, B., Sutton, R. T., and Scaife, A. A.: Multidecadal modulation of El Niño-Southern Oscillation (ENSO) variance by Atlantic Ocean sea surface temperatures, Geophys. Res. Lett., 33, L08705, doi:10.1029/2006GL025766, 2006.

Feliks, Y. M., Ghil, M., and Robertson, A. W.: The atmospheric circulation over the North Atlantic as induced by the SST field, J. Climate, 24, 522-542, 2011.

Fyke, J., Weaver, A. J., Pollard, D., Eby, M., Carter, L., and Mackintosh, A.: A new coupled ice sheet/climate model: description and sensitivity to model physics under Eemian, Last Glacial Maximum, late Holocene and modern climate conditions, Geosci Model Dev Discuss, 4, 117-136, 2011.

Grinsted, A., Moore, J. C., and Jevrejeva, S.: Application of the cross wavelet transform and wavelet coherence to geophysical time series, Nonlinear Processes in Geophysics, 11, 561-566, 2004.

Hewitt, C., and Mitchell, J.: A fully coupled general circulation model simulation of the climate of the mid-Holocene, Geophys Res Lett, 25, 361-364, 1998.

Jackson, C. S., and Broccoli, A. J.: Orbital forcing of Arctic climate: mechanisms of climate response and implications for continental glaciation, Clim Dyn, 21, 539-557, 2003.

Kutzbach, J. E.: Monsoon climate of the early Holocene: Climate experiment with the Earth's orbital parameters for 9000 years ago, Science, 214, 59-61, 1981.

Kutzbach, J. E., Liu, X. D., and Liu, Z. Y.: Simulation of the evolutionary response of global summer monsoons to orbital forcing over the past 280,000 years, Clim Dyn, 30, 567-579, 2008.

Li, Z. Q., Sun, J. Y., Hou, S. G., Tian, L. D., and Liu, B. Z.: Glaciochemistry and its environmental significance, in: Glaciers and Their Environments in China - the Present, Past and Future, edited by: Shi, Y. F., Science Press, Beijing, 411, 132-160, 2000.

Liu, Z., Wang, Y., Gallimore, R., Notaro, M., and Prentice, I. C.: On the cause of abrupt vegetation collapse in North Africa during the Holocene: climate variability vs. vegetation feedback, Geophys Res Lett 33, L22709, doi:10.1029/2006GL028062, 2006.

Lorenz, S. J., and Lohmann, G.: Accelerated technique for Milankovitch type forcing in a coupled atmosphere-ocean circulation model: method and application for the Holocene, Clim Dyn, 23, 727-743, 2004.

Matthews, H. D., Weaver, A. J., Meissner, K. J., Gillett, N. P., and Eby, M.: Natural and anthropogenic climate change: Incorporating historical land cover change, vegetation dynamics and the global carbon cycle, Clim. Dyn., 22, 461–479, 2004.

Milankovitch, M.: Canon of insolation and the ice-age problem (Beograd Koniglidh Serbische Akademie, 1941). English translation by the Israel program for scientific translations., US department of Commerce and National Science Foundation, Washington D C, 633 pp., 1969.

Mitchell, T. D., and Jones, P. D.: An improved method of constructing a database of monthly climate observations and associated high-resolution grids, Int. J. Climatology, 25, 693-712, doi: 10.1002/joc.1181, 2005.

Montoya, M., von Storch, H., and Crowley, T.: Climate simulation for 125,000 years ago with a coupled ocean-atmosphere generalcirculation model, J Climate, 13, 1057-1072, 2000.

Schulz, M., and Mudelsee, M.: REDFIT: Estimating red-noise spectra directly from unevenly spaced paleoclimatic time series, Computers and Geosciences, 28, 421-426, 2002.

Shi, Y. F., Yao, T. D., and Yang, B.: Decadal climatic variations recorded in Guliya ice core and comparison with the historical documentary data from East China during the last 2000 years, Science in China (Series D), 29, 79-86, 1999.

Short, D. A., mengel, J. G., and Crowley, T. J.: Filtering of Milankovitch cycles by Earth's geography, Quaternary Research, 35(2), 157-173, 1991.

Stouffer, R. J., Yin, J., Gregory, J. M., Dixon, K. W., Spelman, M. J., Hurlin, W., Weaver, A. J., Eby, M., Flato, G. M., Hasumi, H., Hu, A., Jungclause, J. H., Kamenkovich, I. V., Levermann, A., Montoya, M., Murakami, S., Nawrath, S., Oka, A., Peltier, W. R., Robitaille, D. Y., Sokolov, A., Vettoretti, G., and Weber, S. L.: Investigating the causes of the response of the thermohaline circulation to past and future climate changes, Journal of Climate, 19, 1365-1387, 2006.

Sutton, R. T., and Hodson, D. L. R.: Atlantic Ocean forcing of North American and European summer climate, Science, 309, 115-118, 2005.

Timm, O., and Timmermann, A.: Simulation of the Last 21 000 Years Using Accelerated Transient Boundary Conditions, J Climate, 20, 4377-4401, 2007.

Timmermann, A., Lorenz, S. J., An, S. I., Clement, A., and Xie, S. P.: The effect of orbital forcing on the mean climate and variability of the tropical Pacific, J Climate, 20, 4147-4159, doi:10.1175/jcli4240.1, 2007.

Wang, Y., Li, S., and Luo, D.: Seasonal response of Asian monsoonal climate to the Atlantic Multidecadal Oscillation, J Geophys Res, 114, D02112, doi:10.1029/2008JD010929, 2009.

Weaver, A. J., Eby, M., Wiebe, E. C., Bitz, C. M., Duffy, P. B., Ewen, T. L., Fanning, A. F., Holland, M. M., MacFadyen, A., Matthews, H. D., Meissner, K. J., Saenko, O., Schmittner, A., Wang, H., and Yoshimori, M.: The UVic Earth System Climate Model: Model description, climatology, and applications to past, present and future climates, Atmosphere-Ocean, 39, 1–68, 2001.

Weber, S., Drijfhout, S., Abe-Ouchi, A., Crucifix, M., Eby, M., Ganopolski, A., Murakami, S., Otto-Bliesner, B., and Peltier, W.: The modern and glacial overturning circulation in the Atlantic ocean in PMIP coupled model simulations, Climate of the Past, 3, 51-64, 2007.

Weldeab, S., Lea, D. W., Schneider, R. R., and Andersen, N.: 155,000 Years of West African Monsoon and Ocean Thermal Evolution Science 316, 1303-1307, doi:10.1126/science.1140461, 2007.

Xiao, D., Zhou, X., and Zhao, P.: Numerical simulation study of temperature change over East China in the past millennium, Sci China Earth Sci, doi:10.1007/s11430-012-4422-3, 2012.

Yang, Z. H., Yao, T. D., Huang, C. L., and Sun, W. Z.: Younger Drays record in the Guliya ice core, Chin Sci Bull, 42, 1975-1978, 1997.

Yao, T. D., Jiao, K. Q., Li, Z. Q., Shi, W. L., Li, Y. F., Liu, J. S., Huang, C. L., and Xie, C.: Climatic and environmental records in Guliya Ice Cap, Science in China (Series D), 37, 766-773, 1994.

Yao, T. D., Thompson, L. G., and Jiao, K. Q.: Recent warming as recorded in the Qinghai-Tibetan cryosphere, Annals of Glaciology, 21, 196-200, 1995.

Yao, T. D., Lonnie, G., Thompson, E. M., Yang, Z., Zhang, X., and Lin, P. N.: Climatological significance of $\delta^{18}O$ in the north Tibetan ice cores, J Geophys Res, 101(D23), 29531-29537, 1996a.

Yao, T. D., Qin, D. H., Tian, L. D., Jiao, K. Q., Yang, Z. H., and Xie, C.: Variations in temperature and preipitation in the past 2000 years on the Xizang (Tibet) Plateau—Guliya ice core record, Science in China (Series D), 26, 348-353, 1996b.

Yao, T. D., Thompson, L. G., Shi, Y. F., Qin, D. H., Jiao, K. Q., Yang, Z. H., Thompson, E. M., and Tian, L. D.: Climate variation since the Last Interglaciation recorded in the Guliya ice core, Science in

China (Series D), 40, 447-452, 1997.
Yao, T. D., and Wang, N. L.: Past, now and future of the ice core study, Chinese Science Bulletin, 42 (3), 225-230, 1997.
Yao, T. D., Wang, N. L., and Shi, Y. F.: Climate and entironmental changes recorded in the ice cores, in: Glaciers and Their Environments in China - the Present, Past and Future, edited by: Shi, Y. F., Science Press, Beijing, 411, 285-319, 2000.
Yao, T. D., Xu, B. Q., and Pu, J. C.: Climatic changes on orbital and sub-orbital time scale recorded by the Guliya ice core in Tibetan plateau, Science in China (Series D), 31, 287-294, 2001.
Yin, Q. Z., and Berger, A.: Insolation and CO2 contribution to the interglacial climate before and after the Mid-Brunhes Event, Nature Geoscience, 3, 243 - 246, 2010.
Yin, Q. Z., and Berger, A.: Individual contribution of insolation and CO2 to the interglacial climates of the past 800,000 years, Climate Dynamics, 38, 709-724, 2012.
Zhang, X., Shi, Y. F., and Yao, T. D.: Variational features of precipitation δ~(18)O in Northeast Qinghai-Tibet Plateau, Science in China (Series D), 25(5), 540-547, 1995.

Figure Legends

Fig. 1. Annual cycles of (a) incoming solar radiation anomalies and (b) simulated Guliya SAT anomalies relative to the climatological mean over the past 130 ka. The abscissa is time before the present, and the ordinate is the month of a year.

Fig. 2. Correlation coefficients (open squares) between the Guliya $\delta^{18}O$ and the simulated Guliya monthly mean SAT during the 1308 model years. The horizontal short-dashed and long-dashed lines indicate the 95% and 99% confidence levels, respectively.

Fig. 3. Time series of the simulated Guliya August–September SAT (red line; left ordinate) and the Guliya $\delta^{18}O$ (green line; right ordinate). The correlation coefficient (R) between them is 0.47, significant at the 99.9% confidence level.

Fig. 4. Power spectrum of the Guliya $\delta^{18}O$.

Fig. 5. Squared wavelet coherence between the simulated August–September Guliya SAT and the Guliya $\delta^{18}O$. The 5% significance level against red noise is shown as a thick line. The arrow points rightward for an in-phase relationship and points leftwards for an anti-phase relationship.

Fig. 6. Composite differences in the simulated August–September SAT between the

warm and cold phases of the Guliya August–September SAT, in which the time of the warm and cold phases is indicated above each panel. The shaded areas represent the values significant at the 95% confidence level.

Fig. 7. Simulated August–September Guliya SAT (green; right ordinate) and obliquity (purple; left ordinate) in the past 130 ka.

Fig. 8. Annual cycles of the Guliya SAT in the warm (closed circles) and cold phases (open squares) of the August–September Guliya SAT and their difference (warm phase minus cold phase; open circle). The time of the warm and cold phases is indicated in each panel.

Fig. 9. Same as in Fig. 6 but for SST.

Fig. 10. Correlation coefficients between the Guliya $\delta^{18}O$ and the simulated August–September SAT during the 1308 model years. The shading indicates the correlation coefficients significant at the 95% confidence level.

Fig. 11. Same as in Fig. 10 but for the correlation between the Guliya $\delta^{18}O$ and the simulated August–September SST.

Fig. 12. Leading and lagging correlation coefficients (solid lines) between the

simulated Guliya August–September SAT and (a) the North Atlantic (60°W–0°W, 50°–70°N) August–September SST and (b) the Guliya August–September precipitation. The horizontal short-dashed lines represent the 95% confidence level.

Fig. 13. The simulated August–September Guliya SAT (green; right ordinate) and precipitation (red; left ordinate).

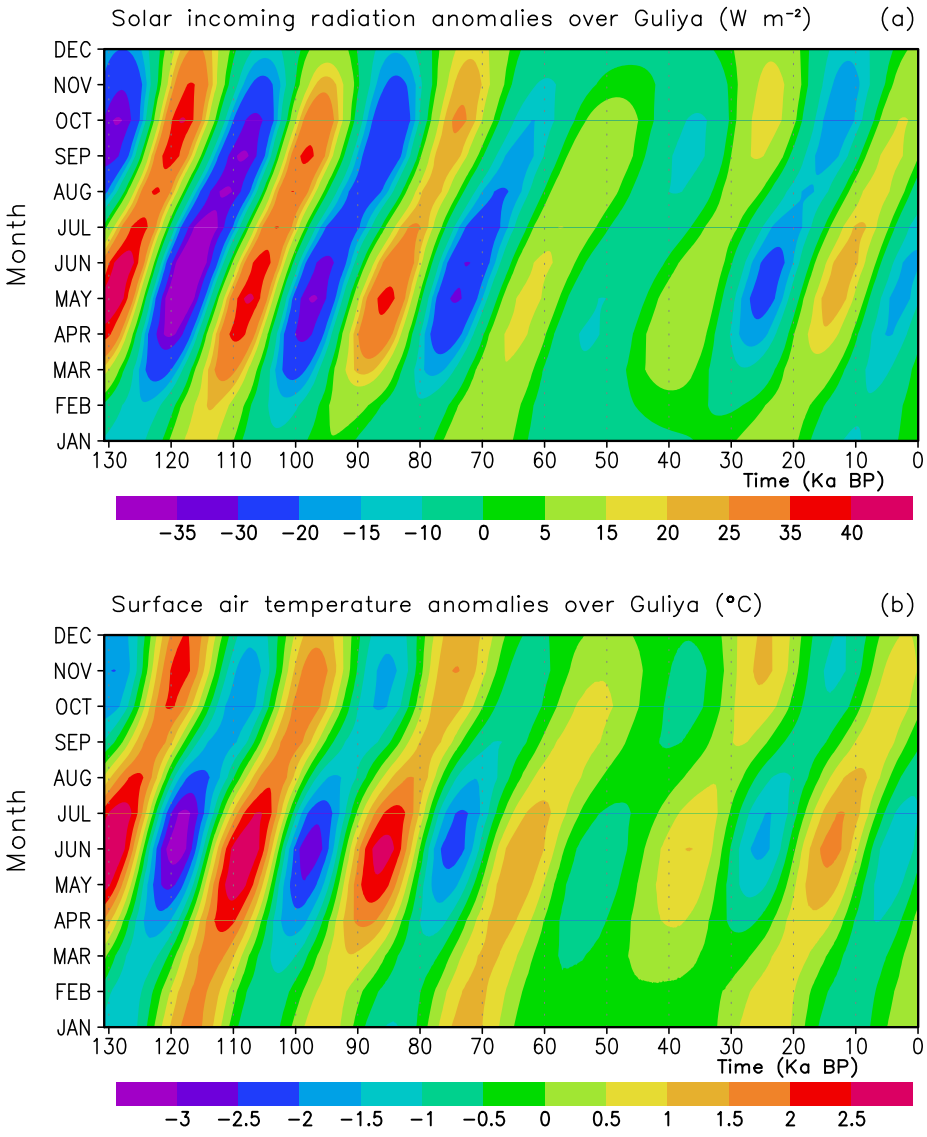

Fig. 1. Annual cycles of (a) incoming solar radiation anomalies and (b) simulated Guliya SAT anomalies relative to the climatological mean over the past 130 ka. The abscissa is time before the present, and the ordinate is the month of a year.

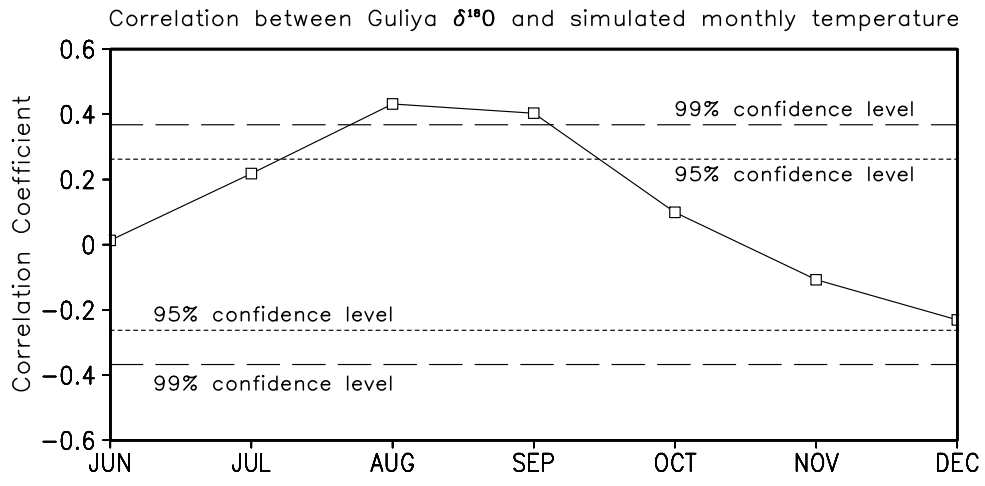

Fig. 2. Correlation coefficients (open squares) between the Guliya $\delta^{18}O$ and the simulated Guliya monthly mean SAT during the 1308 model years. The horizontal short-dashed and long-dashed lines indicate the 95% and 99% confidence levels, respectively.

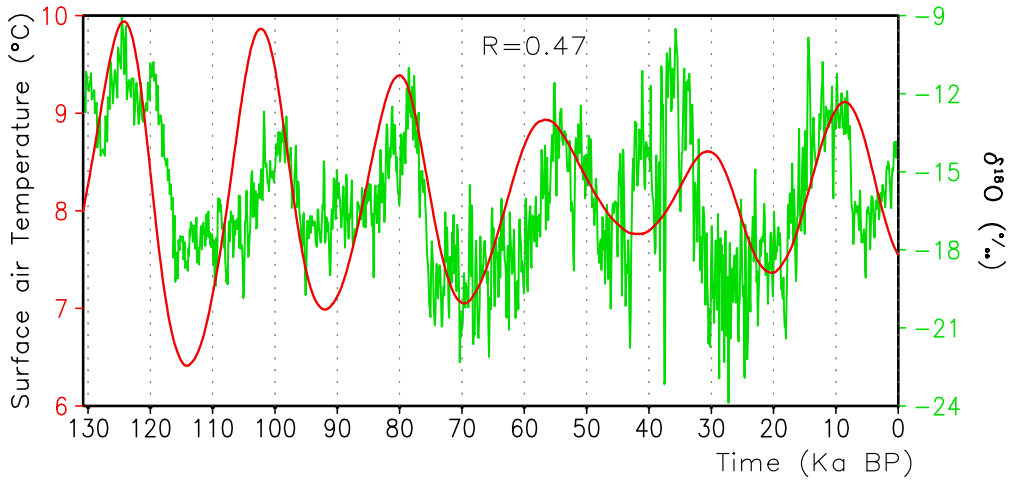

Fig. 3. Time series of the simulated Guliya August–September SAT (red line, left ordinate) and the Guliya $\delta^{18}O$ (green line, right ordinate). The correlation coefficient (R) between them is 0.47, significant at the 99.9% confidence level.

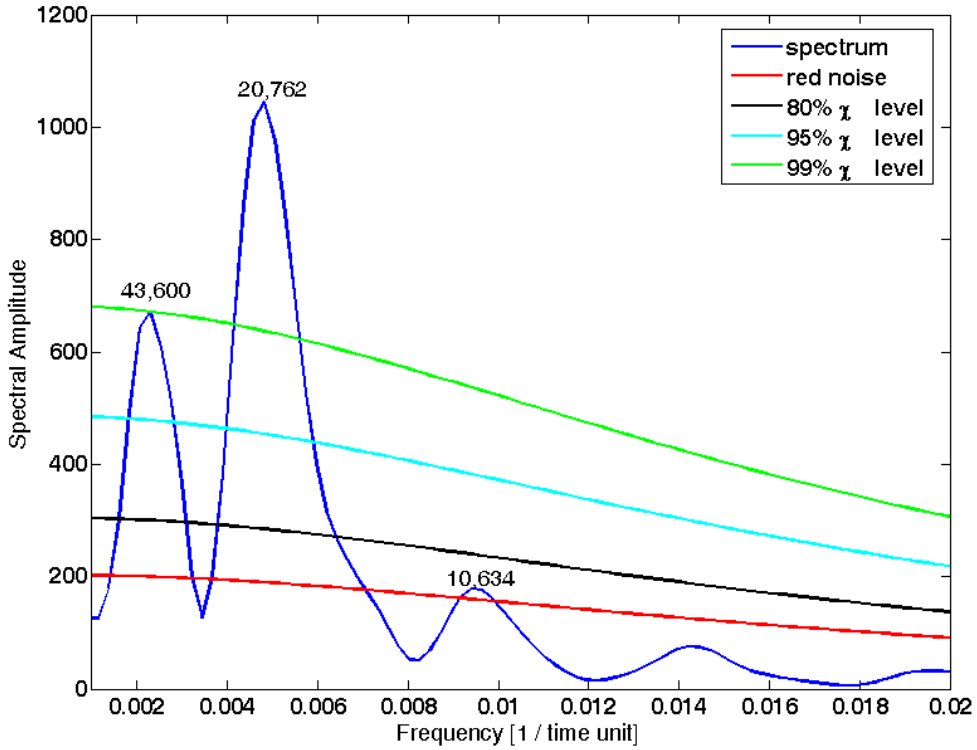

Fig. 4. Power spectrum of the Guliya $\delta^{18}O$.

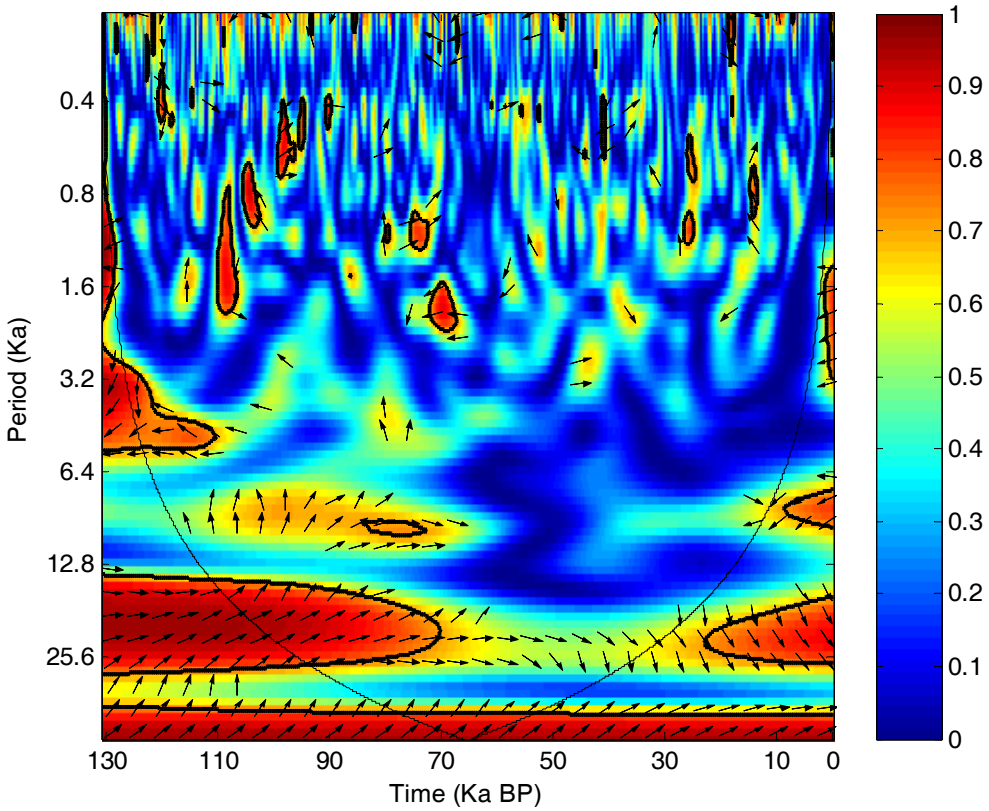

Fig. 5. Squared wavelet coherence between the simulated August–September Guliya SAT and the Guliya $\delta^{18}O$. The 5% significance level against red noise is shown as a thick line. The arrow points rightward for an in-phase relationship and points leftwards for an anti-phase relationship.

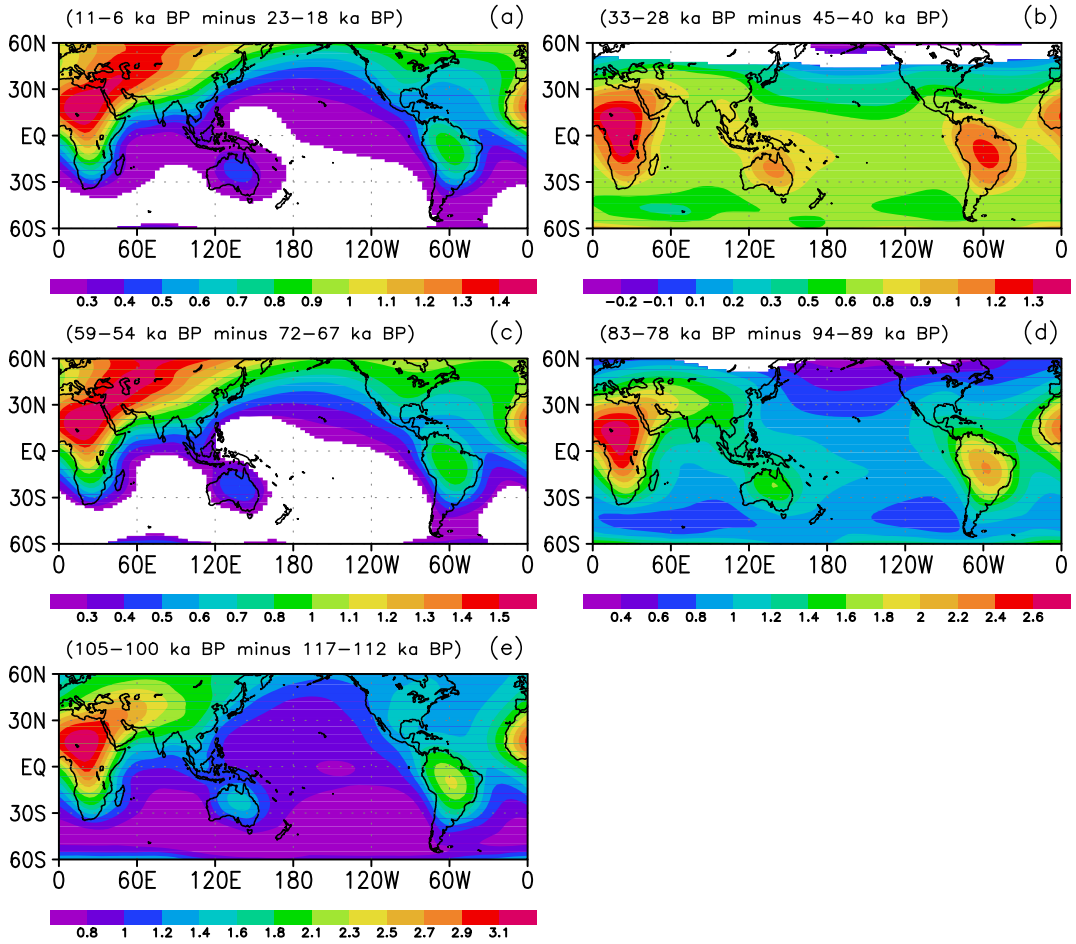

Fig. 6. Composite differences in the simulated August–September SAT between the warm and cold phases of the Guliya August–September SAT, in which the time of the warm and cold phases is indicated above each panel. The shaded areas represent the values significant at the 95% confidence level.

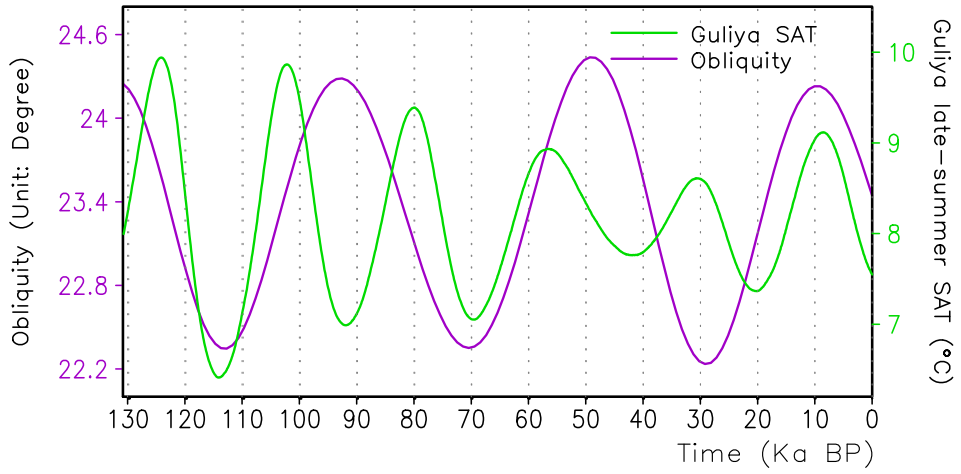

Fig. 7. Simulated August–September Guliya SAT (green; right ordinate) and obliquity (purple; left ordinate) in the past 130 ka.

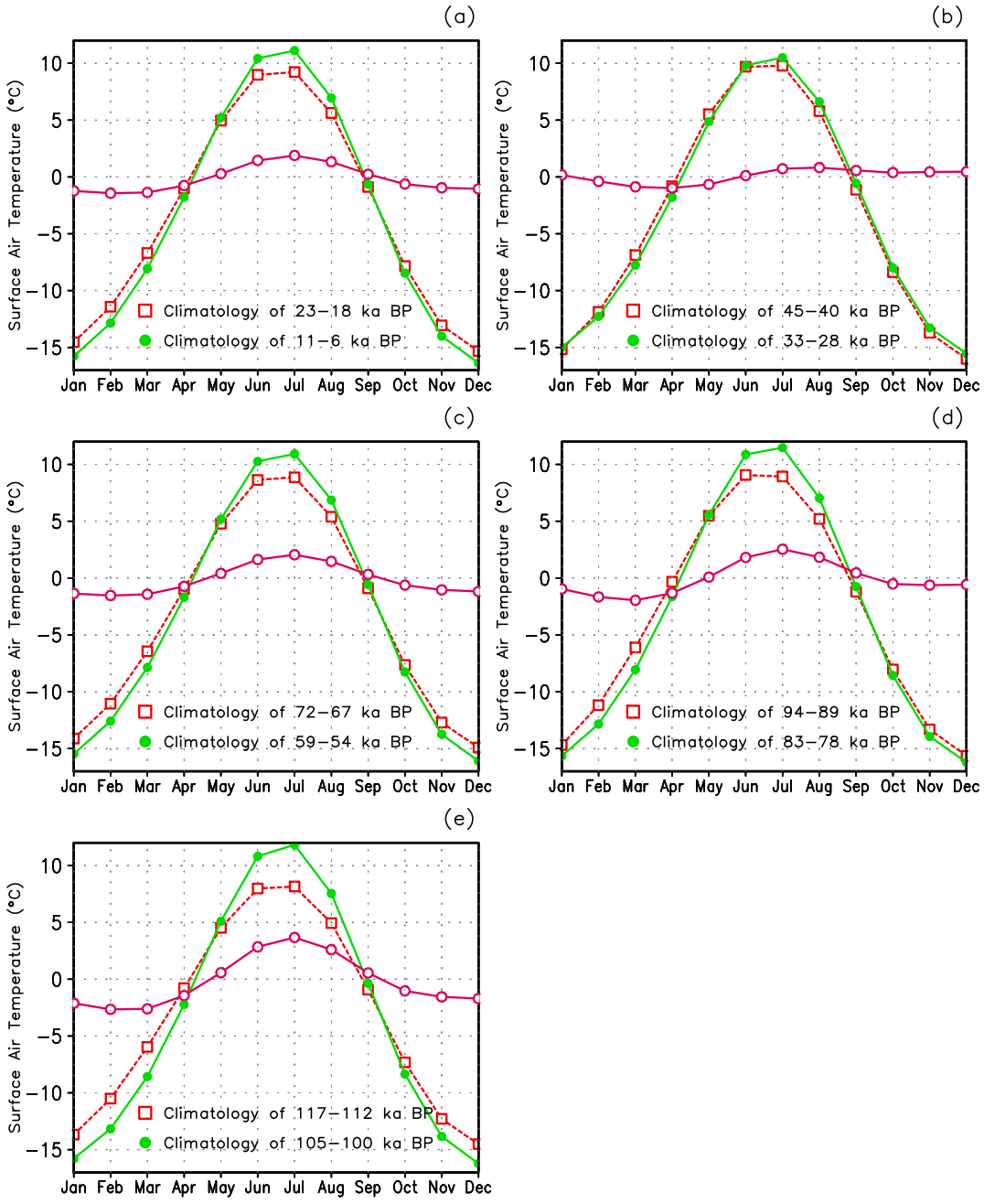

Fig. 8. Annual cycles of the Guliya SAT in the warm (closed circles) and cold phases (open squares) of the August–September Guliya SAT and their difference (warm phase minus cold phase; open circle). The time of the warm and cold phases is indicated in each panel.

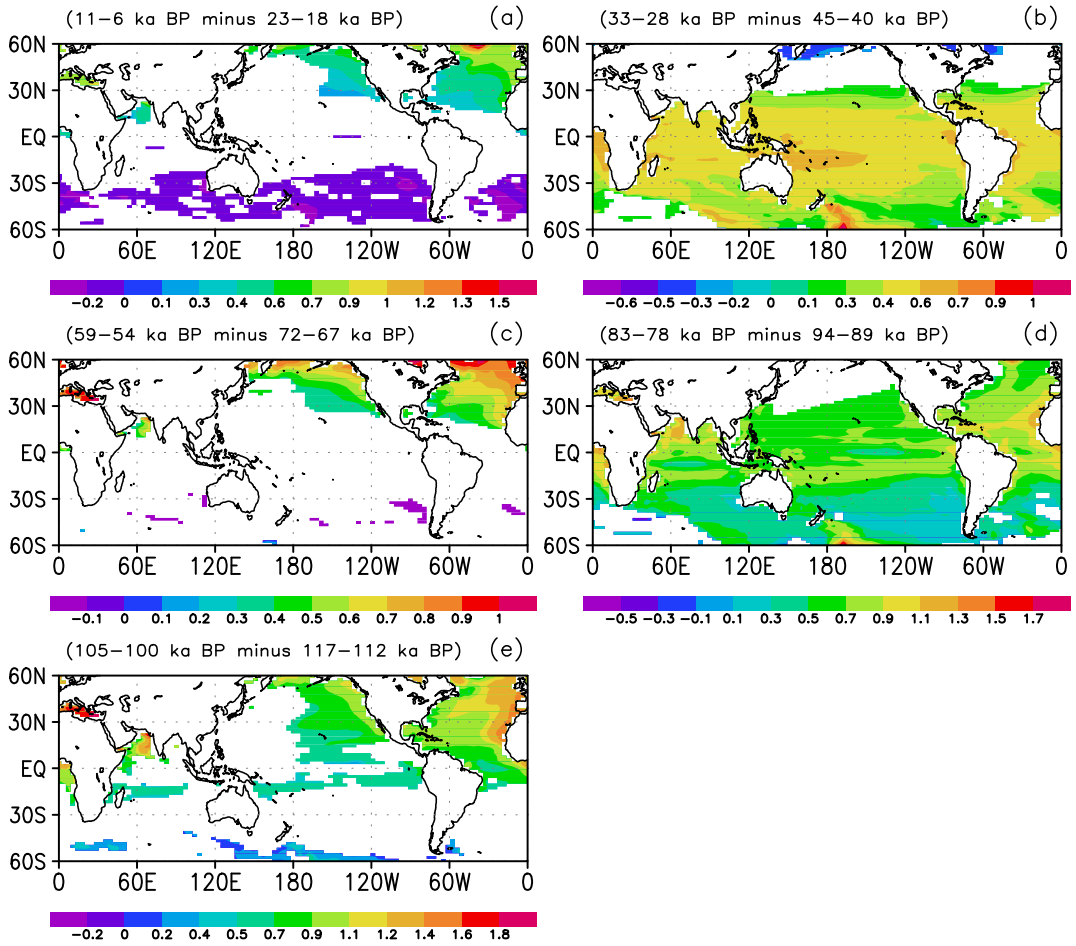

Fig. 9. Same as in Fig. 6 but for SST.

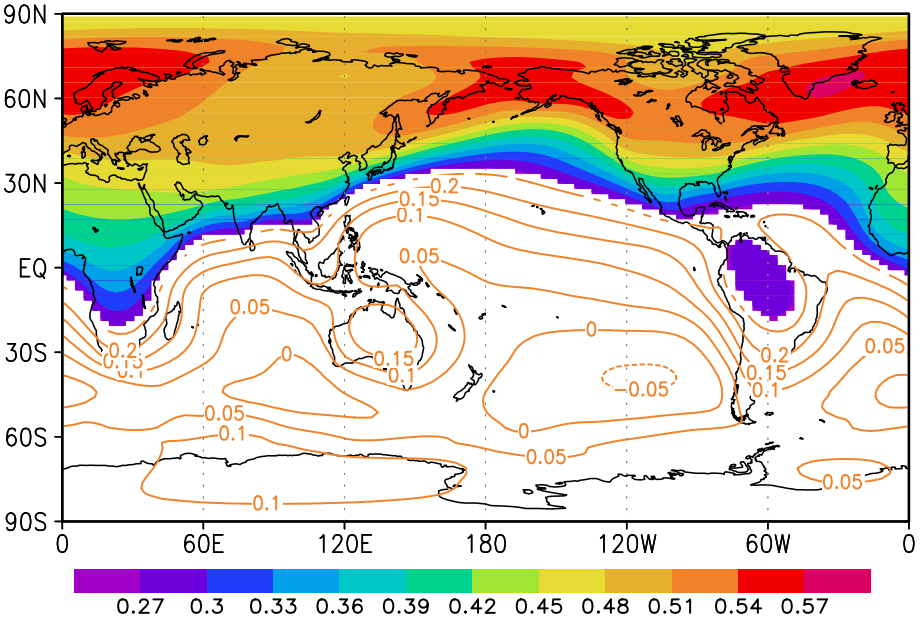

Fig. 10. Correlation coefficients between the Guliya $\delta^{18}O$ and the simulated August–September SAT during the 1308 model years. The shading indicates the correlation coefficients significant at the 95% confidence level.

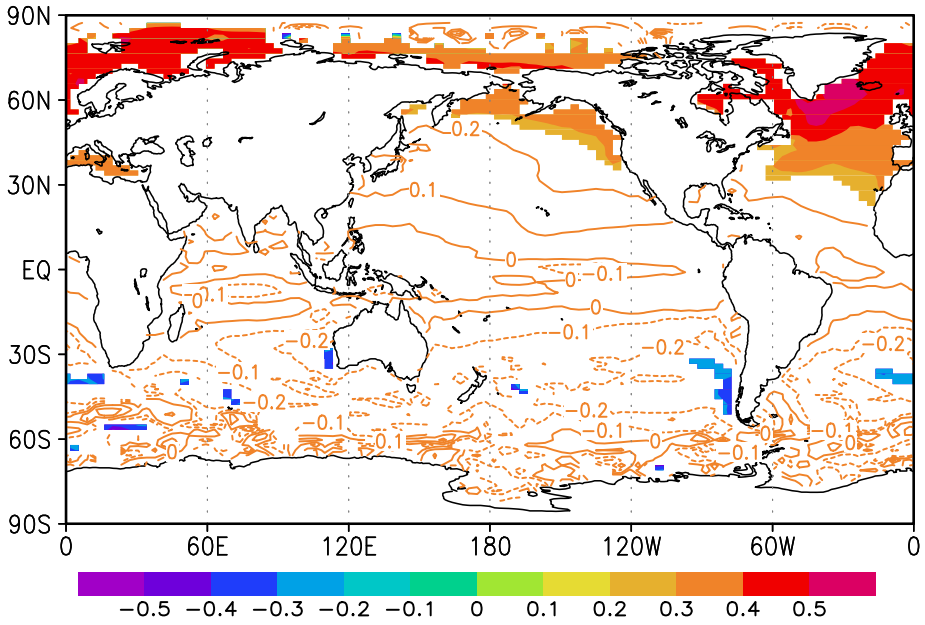

Fig. 11. Same as in Fig. 10 but for the correlation between the Guliya $\delta^{18}O$ and the simulated August–September SST.

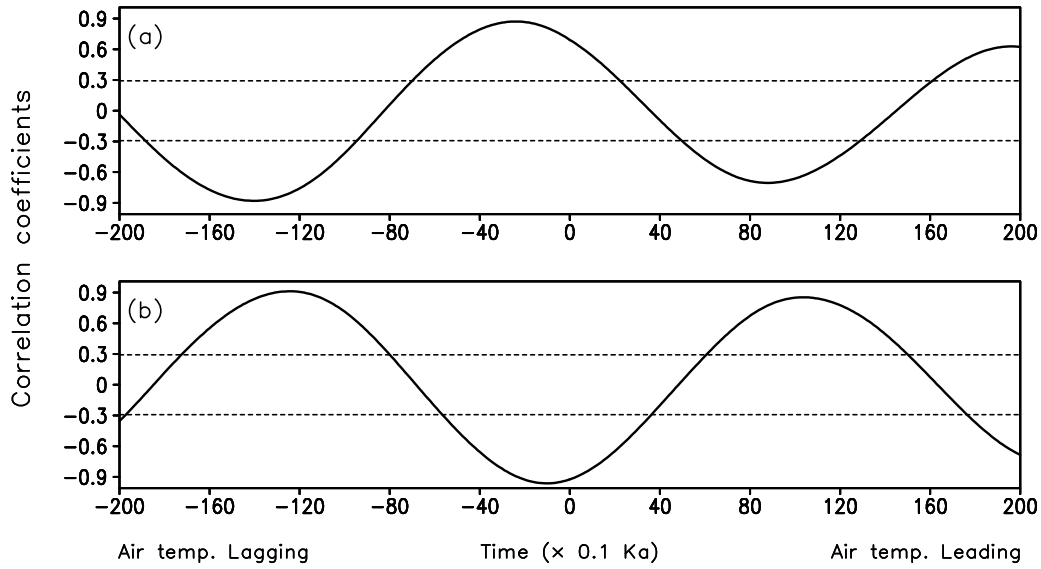

Fig. 12. Leading and lagging correlation coefficients (solid lines) between the simulated Guliya August–September SAT and (a) the North Atlantic (60°W–0°W, 50°–70°N) August–September SST and (b) the Guliya August–September precipitation. The horizontal short-dashed lines represent the 95% confidence level.

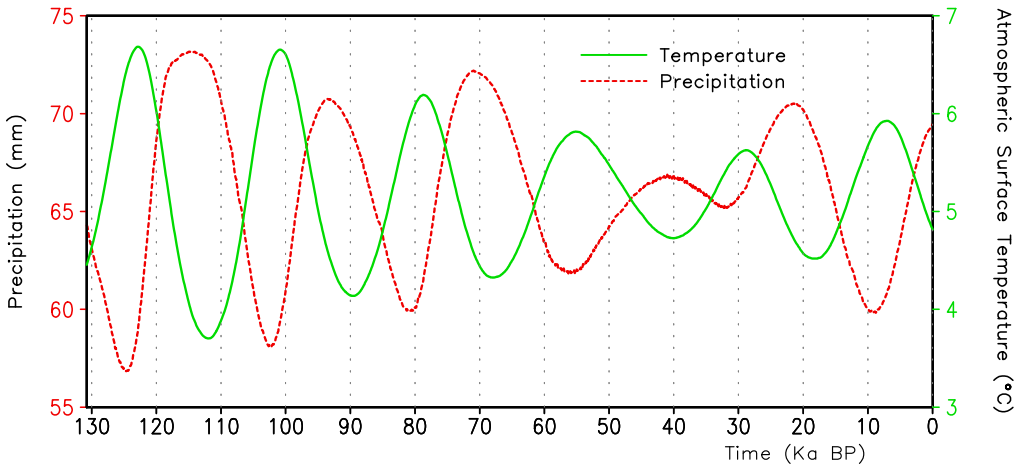

Fig. 13. The simulated August–September Guliya SAT (green; right ordinate) and precipitation (red; left ordinate).